

## Article

# Criticality for Oblique Detonation Waves Induced by a Finite Wedge in a Hydrogen–Air Mixture

Jianxiu Qin \* and Dehua Zhu

China Academy of Aerospace Aerodynamics, Beijing 100074, China

\* Correspondence: qinjianxiu@hotmail.com

**Abstract:** Two-dimensional oblique detonation waves (ODWs) induced by finite wedges in a stoichiometric hydrogen–air mixture have been investigated numerically based on reactive Euler equations with a detailed chemical reaction model. The main zone affected by the expansion wave emanating from the turning point of a wedge is the flowfield downstream of the intersection point of the oblique shock wave (OSW) and the expansion wave. The ODW would be reduced to Chapman–Jouguet (CJ) detonation or decoupled combustion downstream. Three combustion regimes, detonation, decoupled combustion, and no ignition, were observed successively, as the wedge length decreases. It is found that the location of the intersection point is a key parameter for the detonation initiation. When the intersection point is located upstream of the ODW transition point, the expansion wave may quench ODW. Then, the critical wedge length is obtained by theoretical analysis of wave structures and the initiation criterion of ODWs for finite wedges is proposed. When the wedge length is greater than the critical wedge length, ODWs can be initiated. On the contrary, the initiation of ODWs do not occur. For wedge lengths small enough, no ignition occurs. Previously proposed criteria that use the induction length are also examined and compared with the present critical wedge length criterion in this study, and the latter is proven to achieve better results.

**Keywords:** oblique detonation; finite wedge; initiation; expansion wave



**Citation:** Qin, J.; Zhu, D. Criticality for Oblique Detonation Waves Induced by a Finite Wedge in a Hydrogen–Air Mixture. *Aerospace* **2023**, *10*, 508. <https://doi.org/10.3390/aerospace10060508>

Academic Editor: James ‘Chris’ Thomas

Received: 30 April 2023

Revised: 23 May 2023

Accepted: 24 May 2023

Published: 27 May 2023



**Copyright:** © 2023 by the authors. Licensee MDPI, Basel, Switzerland. This article is an open access article distributed under the terms and conditions of the Creative Commons Attribution (CC BY) license (<https://creativecommons.org/licenses/by/4.0/>).

## 1. Introduction

Detonation-based engines are attracting increased attention for their high thermal cycle efficiency [1–4]. One type of engine is the oblique detonation wave engine (ODWE) based on oblique detonation waves (ODWs), which is suitable for air-breathing propulsion systems at high Mach numbers. In this engine, a combustible mixture flows through an oblique wedge with a velocity exceeding the CJ speed, and a stable detonation is formed. The combustion can be completed in a short distance, and thus the combustor length can be shortened, which enables structure simplification and mitigates cooling problems. In addition, oblique detonations are initiated in high Mach number flow, broadening the range of flight Mach numbers. Therefore, the ODWE is an innovative engine that could be used for future aircraft.

However, there are many challenges that need to be addressed in order to realize this potential propulsion system ODWE. The initiation and structure of ODWs need to be clarified first. In early research, ODWs were simplified into oblique shock waves (OSWs) with a heat release zone attached to the wedge [5,6]. The relationship between inflow parameters and oblique shock/detonation properties can be determined by shock polar analysis [7–9]. Li et al. [10], numerically investigated an oblique detonation and found that it was composed of a nonreactive OSW, an induction region, a set of deflagration waves, and the detonation surface. The transition from the OSW to a detonation was achieved by a multi-wave point. Later, Vlasenko et al. [11] observed a smooth OSW to an oblique detonation transition. These two structures were confirmed in the experiments in [12,13] and regarded as the standard structures. Silva and Deshaies [14] conducted a

parametric study on ODWs and observed both abrupt and smooth OSW–ODW transitions. The criterion condition for the transition structures of ODWs was first proposed. Teng et al. [15] put forward a criterion based on the difference between the detonation and OSW angles, which was more applicative in the cases with different inflow conditions. Furthermore, other criteria [16–18] based on velocities have also been proposed in recent years. Shi et al. [19] proposed a theoretical criterion, depending on the ratio of the height of the compression wave intersection point and the corresponding height of OSW at the same  $x$ -location, which was applicable to hydrocarbon fuel-based mixtures. For abrupt oblique detonation, several complex wave structures in the initiation region have been observed in cases with large wedges and low incident Mach numbers: for example, the  $\lambda$ -shaped shock, X-shaped shock, Y-shaped shock, and a secondary ODW [20–24]. Teng et al. [25] analyzed four morphological features in the initiation region by Mach lines and the Mach number ratio of Mach number in the induction zone and the corresponding CJ Mach number. Then, a non-dimensional Damköhler number  $Da_s$  was defined to quantify the flow/reaction. A strong peak of  $Da_s$  was observed in the abrupt transition, while a bump was observed in the smooth transition [26].

The above studies focused on ODWs induced by an infinite wedge. For real ODWs, detonation is produced in a confined space, in which expansion waves would emanate from the upper-wall turning point and the wedge turning point. A complicated ODW morphology was observed considering the interaction between the ODW and the expansion wave from the upper wall [27]. The expansion wave derived from the wedge turning point may quench the ODW [28,29]. Walter and Silva [30] found that a CJ ODW was obtained for intermediate wedge angles, and the decoupling of the ODW was observed for wedge angles near the maximum attach angle. Fang et al. [31] investigated the effects of expansion waves on the two initiation mechanisms of ODWs and found that the structure of the wave-controlled initiation was more sensitive to the expansion waves than the kinetic-controlled initiation. The effects of equivalence ratios, wedge angle and Mach numbers on the initiation mode were studied [32,33]. Xiang et al. [34] proposed the initiation criterion of ODWs for finite wedges. When the characteristic length of the induction zone is less than the characteristic length of the oblique wedge, the initiation of ODW occurs. However, Liu et al. [35] obtained stable, prompt ODWs with a wedge length smaller than the induction length. Thus, the effect of the expansion wave on the initiation of ODW is still not explained clearly.

In this paper, wave structures of ODWs induced by finite wedges are numerically investigated based on 2D reactive Euler equations with detailed chemistry reaction models. In Section 2, physical and numerical models are introduced. In Section 3, the effects of the expansion wave on wave structures are analyzed, and the initiation criterion for finite wedge-induced ODWs is proposed and verified. Concluding remarks are given in Section 4.

## 2. Physical and Numerical Models

### 2.1. Physical Model

Figure 1 presents the computational domain and sketch of an oblique detonation wave induced by an infinite wedge and a finite wedge. The combustible gas mixture with a high incident Mach number hits the oblique wedge and an OSW is generated. The shock wave may induce an exothermic chemical reaction, resulting in an oblique detonation wave (ODW) downstream. The gray zone is the solid wall. For a finite wedge, the wedge contains a ramp and a horizontal wedge. The expansion waves produced at the turning point will influence the flowfield in the vicinity of the horizontal wedge. The computational domain is enclosed by the dashed line and the upper boundary of the gray zone.

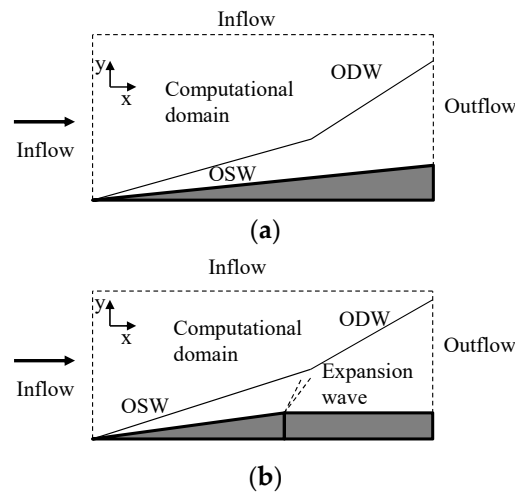


**Figure 1.** Sketch of oblique detonation wave and computational domain. (a) Infinite wedge. (b) Finite wedge.

2.2. Numerical Method

A previous investigation [36] showed that the boundary layer and viscosity had little influence on the ODW structure, and most of the studies were based on inviscid simulations. The governing equations are two-dimensional multi-species reactive Euler equations, written as follows:

$$\frac{\partial U}{\partial t} + \frac{\partial F}{\partial x} + \frac{\partial G}{\partial y} = S \tag{1}$$

where

$$U = \begin{bmatrix} \rho_1 \\ \vdots \\ \rho_n \\ \rho u \\ \rho v \\ \rho e \end{bmatrix}, F = \begin{bmatrix} \rho_1 u \\ \vdots \\ \rho_n u \\ \rho u^2 + p \\ \rho uv \\ (\rho e + p)u \end{bmatrix}, G = \begin{bmatrix} \rho_1 v \\ \vdots \\ \rho_n v \\ \rho v^2 + p \\ \rho uv \\ (\rho e + p)v \end{bmatrix}, S = \begin{bmatrix} \dot{\omega}_1 \\ \vdots \\ \dot{\omega}_2 \\ 0 \\ 0 \\ 0 \end{bmatrix} \tag{2}$$

where  $p$  is the gas pressure, and  $u$  and  $v$  are the velocities in the  $x$ -direction and  $y$ -direction, respectively.  $\rho_i$  is the  $i$ th species density and the total density  $\rho = \sum_i^n \rho_i$ ;  $e$  is the total energy, calculated by; total  $e = h - \frac{p}{\rho} + \frac{1}{2}(u^2 + v^2)$  enthalpy  $h$  can be written as  $h = \sum_{i=1}^n \rho_i h_i / \rho$  and the  $i$ th species specific enthalpy can be obtained from thermodynamic data. The equation of the state is

$$p = \sum_{i=1}^n \rho_i R_i T \tag{3}$$

where  $T$  is the gas temperature and  $R_i$  is the  $i$ th species gas constant.  $\omega_i$  is the  $i$ th species mass production rate, which is calculated by a chemical model. Balakrishnam and Willams' [37] chemical reaction model with 9 species ( $O_2, N_2, H, OH, O, H_2, H_2O, HO_2, H_2O_2$ ) and 21 elementary reversible reactions was employed, which has been used to simulate OSW-ODW transitions [12,29]. The chemical mechanism may affect the initiation of the ODW [38], but it is not discussed in this paper. This paper focused on the effects of the expansion wave on the initiation of ODW, and thus the same chemical mechanism was applied in all the cases. The finite volume method (FVM) was used for spatial discretization, while the AUSM + scheme was adopted for the convective fluxes. The left and top boundary were inflow boundaries, in which the static pressure, temperature and Mach number of the inflow were given. The right boundary was the outflow boundary, in which all flow parameters were interpolated under the assumption of the zero first-order derivatives. Slip wall conditions were used on the wedge. The inflow temperature  $T_0$  and

Mach number  $Ma_0$  were 350 K and 6.5. The pressure  $P_0$  was 12.25 kPa. The wedge angle  $\theta$  was fixed at  $30^\circ$ . The inflow combustible gas was a hydrogen–air premixed mixture with  $H_2:O_2:N_2 = 2:1:3.76$ .

### 3. Results and Discussion

#### 3.1. Resolution Study

A uniform mesh in both directions is used in all of the simulations presented in this paper. To verify the grid convergence,  $50\ \mu\text{m}$  and  $25\ \mu\text{m}$  are adopted in a finite wedge case. A finite wedge-induced ODW with two grid resolutions is presented in Figure 2, and the difference in the structure of ODWs can be neglected. For better illustration, the temperature and OH mass fraction along  $y = 15\ \text{mm}$  and  $y = 20\ \text{mm}$  are also depicted in Figure 3. Obviously, the distribution of temperature and OH are similar to each other, although some slight differences can be observed in Figure 3. Therefore, for the purposes of this paper, the chosen grid size of  $50\ \mu\text{m}$  is sufficient to provide a converged global formation structure, guaranteeing the reliability of our conclusions. Nevertheless, a higher resolution is desirable to resolve small-scale details of the cellular structure, a task which is outside the scope of this paper.

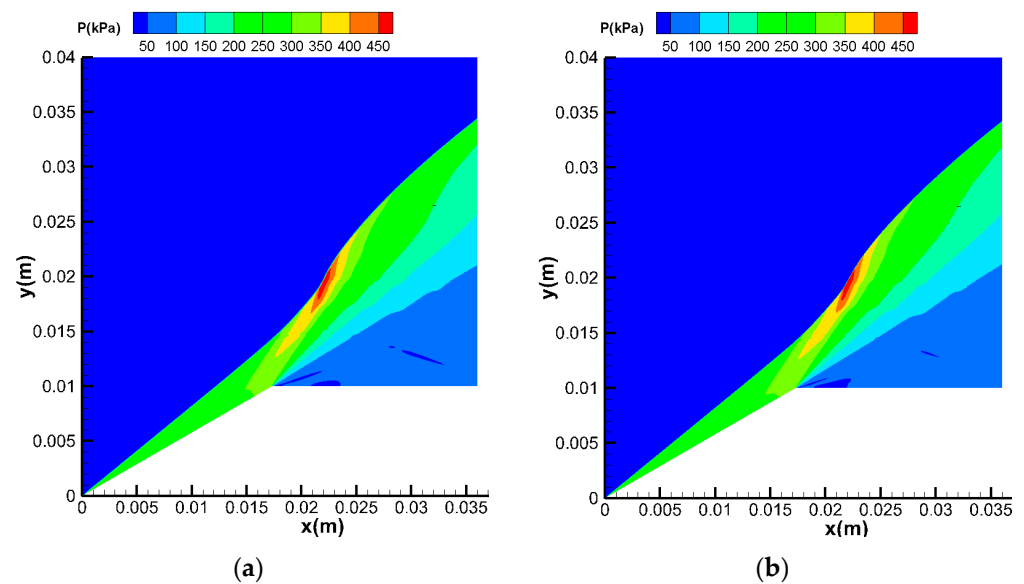


**Figure 2.** Pressure of ODW structures for a finite wedge with different resolutions: (a)  $50\ \mu\text{m}$ ; (b)  $25\ \mu\text{m}$ .

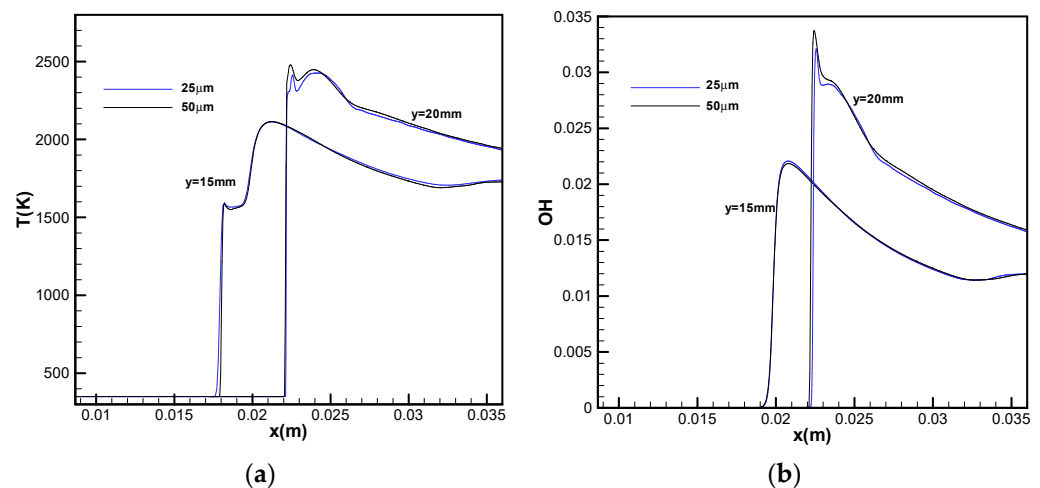


**Figure 3.** Temperature and OH mass fraction for a finite wedge with different resolutions. (a) Temperature. (b) OH.

### 3.2. Effects of Expansion Waves on ODWs

The basic ODW structure induced by the infinite wedge is presented in Figure 4. Figure 4a displays the pressure contour, while Figure 4b presents the temperature contour, and the black lines represent the mass fraction of H<sub>2</sub>O. The OSW is formed in the front of the wedge ( $x = 0$  mm) when the combustible mixtures hit the wedge. The gas pressure and temperature increase sharply behind the OSW, and the auto-ignition of the combustible mixtures occur ( $x = 9$  mm). The deflagration waves converge at the end of the induction zone and interact with the OSW ( $x = 9$  mm–22.5 mm). The angle of the OSW is raised up and the oblique detonation is formed after  $x = 22.5$  mm. The transition from the OSW to the ODW is featured by the curved shock, and thus smooth detonation is triggered. The inflexion point on the curved shock is defined as OSW–ODW transition.

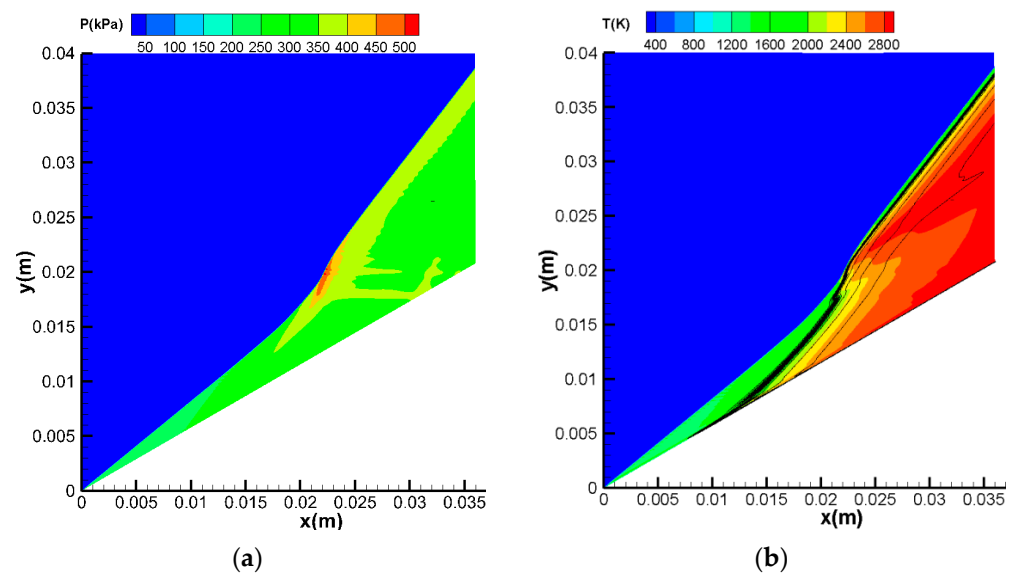


**Figure 4.** Structure of ODW induced by the infinite wedge. (a) Pressure. (b) Temperature and H<sub>2</sub>O mass fraction.

The wedge length is finite in a real ODW engine. Expansion waves would be induced from the turning point of the wedge, which would have an influence on ODW structure. Furthermore, it was found that the locations of expansion waves are changed by the wedge length. Papalexandris [29] concluded that when the triple point occurred downstream of the turning point, the expansion affected the curvature of the leading front and the reaction process. Xiang et al. [34] proposed the following initiation criterion: when the characteristic length of wedge  $L_w$  is larger than the characteristic length of induction zone  $L_c$ , an ODW would be initiated. In this study,  $L_c$  is equal to the length of the front point of the wedge to the front point of the deflagration wave, which is 10.5 mm in the case of the infinite wedge. The OSW–ODW transition point is located at  $x = 22.5$  mm, and its projective length in the wedge is 30 mm. Therefore, the calculated wedge length is from 10 mm to 32 mm. The length of the wedge is defined as the length from the start of the wedge to the end of the wedge, which is marked in Figure 5b.

Figure 5 shows the temperature and H<sub>2</sub>O mass fraction contours of the ODW induced by the 32 mm wedge, 24 mm wedge and 19 mm wedge. Oblique detonations are both initiated successfully at  $x = 22.5$  mm, which indicates that the locations of the OSW–ODW transition remain unchanged. For the 32 mm wedge, the ODW structure is similar to that induced by an infinite wedge. Some differences can be observed, and expansion waves are generated from the turning point. A region with a lower pressure and temperature is formed above the horizontal wedge. However, for the 24 mm wedge and 19 mm wedge, a progressive separation of the H<sub>2</sub>O mass fraction from the shock front occurs at the downstream flow fields. The expansion waves affect the curvature of the shock, which

results in the angles of the shock being smaller than the detonation angle in the infinite case. Furthermore, the angle of the shock in downstream region is decreases as the wedge length decreases from 32 mm to 19 mm. The temperature of combustion products drops below 2500 K due to expansion waves in the 19 mm wedge.

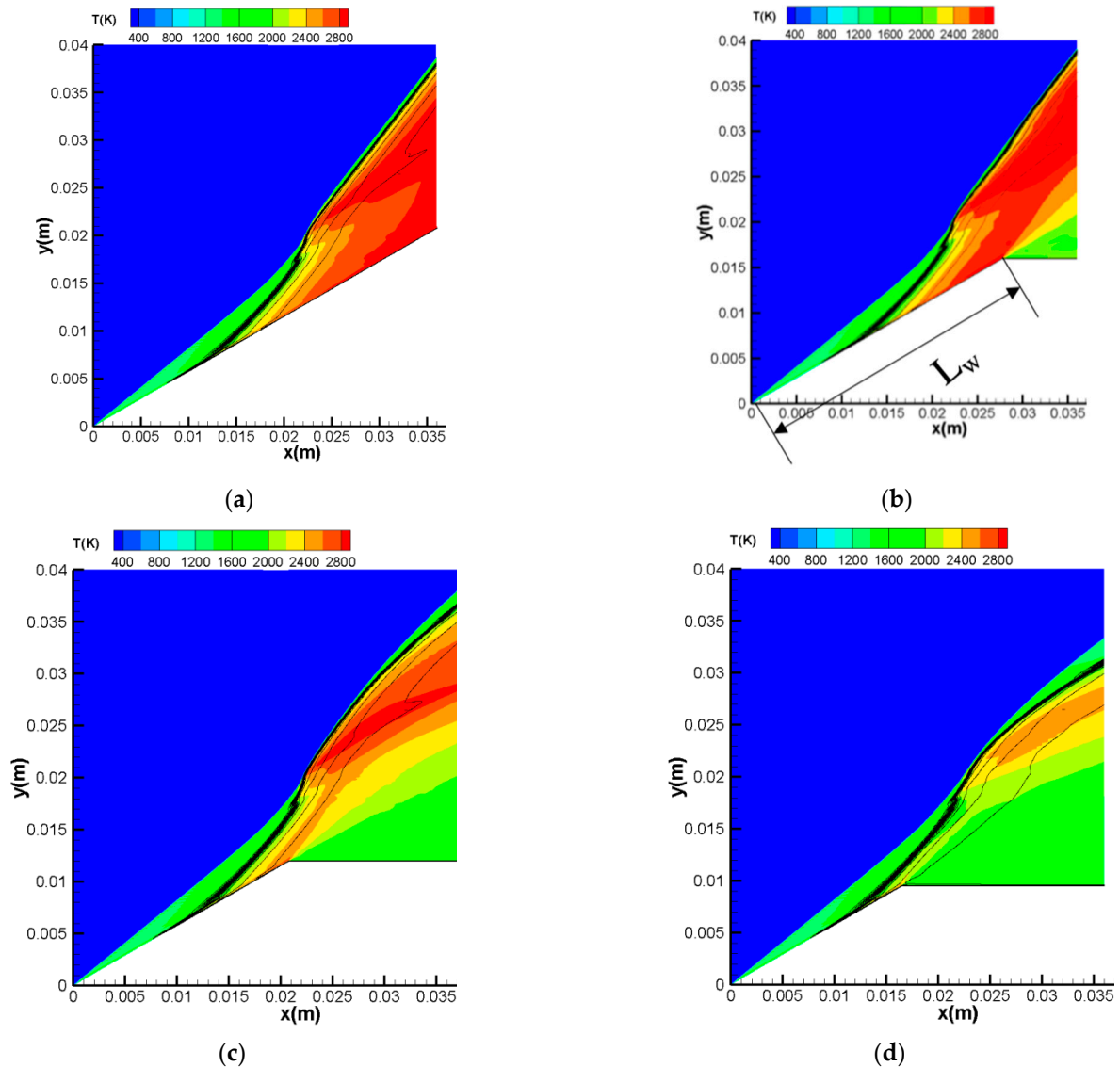


**Figure 5.** Contours of temperature and  $H_2O$  mass fraction (black lines) induced by the infinite wedge, 32 mm wedge, 24 mm wedge and 19 mm wedge: (a) infinite wedge; (b) 32 mm wedge; (c) 24 mm wedge; (d) 19 mm wedge.

Figure 6 shows the pressure and temperature curves along the lines  $y = 12$  mm,  $y = 20$  mm and  $y = 28$  mm of the flow field in Figure 5. These three lines cross the induction zone, transformation point, and detonation zone, respectively. Comparing the pressure and temperature curves in finite wedge cases with those in the infinite wedge case, the region affected by expansion waves and the interaction point of expansion waves and OSW can be established. For  $y = 12$  mm, the pressure and temperature increase sharply at  $x = 14.5$  mm due to the OSW, while the second jump in pressure and temperature is due to the deflagration wave. The red lines for the 32 mm wedge and black line for the infinite wedge almost appear to overlap one another, while the pressure and temperature decrease in the downstream region due to the influence of the expansion waves for the 24 mm wedge and the 19 mm wedge. For  $y = 20$  mm, the pressure increases sharply first

due to the detonation, and then drops to the value in the infinite case. The temperature rises rapidly first and then slowly. For the 32 mm wedge and the 24 mm wedge, the distribution of pressure and temperature in the upstream region is almost the same as that in the infinite case, but the pressure and temperature decrease dramatically at  $x = 30$  mm and  $x = 25$  mm, respectively, which should be attributed to the effects of the expansion waves. For the 19 mm wedge, the peak pressure and temperature are obviously smaller than those in the infinite wedge case. The interaction points of the expansion waves and OSW are near the transition point of ODW. Expansion waves affect the initiation of ODW and the pressure drop rapidly after the shock. For  $y = 28$  mm, the pressure and temperature lines overlap with those for the infinite wedge in the upstream region, but decrease abruptly at  $x = 33$  mm due to the effects of the expansion waves in the 32 mm wedge case. For the 24 mm wedge and 19 mm wedge, the pressure increases as the flow passes through the OSW, but decreases subsequently due to the expansion waves. The OSW in the 19 mm wedge case is located more downstream and the peak pressure is smaller with respect to the other cases, which indicates that the OSWs are weaker with smaller angles.

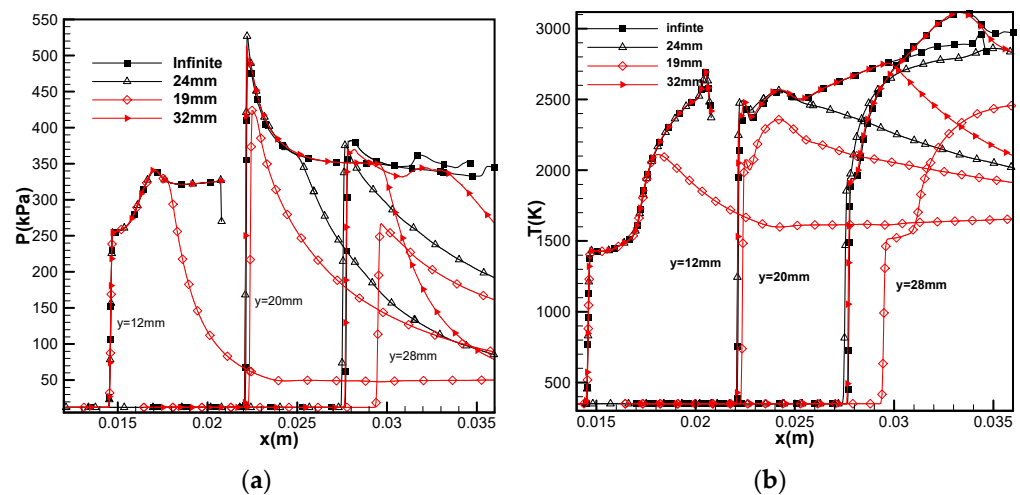


**Figure 6.** Pressure and temperature along  $y = 12$  mm,  $y = 20$  mm and  $y = 28$  mm for the infinite wedge, 32 mm wedge, 24 mm wedge and 19 mm wedge. (a) Pressure. (b) Temperature.

A conclusion can be drawn that the expansion waves affect their downstream flow field, but do not affect their upstream flow field. The structure of the ODW located upstream of the intersection point of the OSW and expansion wave is the same as that in the infinite case, while the shock wave is reduced downstream and the decoupling of the ODW may occur. The expansion waves emanating from the turning point intersect the ODW, which decrease the pressure and reduce the ODW strength, leading to a progressive bending of the ODW. Simultaneously, the temperature downstream of the interaction region is reduced, which leads to an increase in the induction length of the chemical reaction. The induction length would be increased enough to decouple the chemical process from the OSW; thus, the decoupled combustion occurs downstream of the interaction region.

When the wedge length is decreased to 18 mm, the ODW quenches, as shown in Figure 7a. Compared to 19 mm wedge case, the OSW decouples from the reaction front totally, while there exist small zones of detonation in the transition region for 19 mm wedge. As the wedge length decreases, the reaction region and the angle of the shock wave downstream become smaller, as shown in Figure 7b,c. For the 10 mm wedge, the combustible mixtures near the wedge remain almost non-reacted because the temperature is reduced significantly by the expansion waves. A long time is needed for the temperature to increase high enough to trigger a rapid reaction. The reaction should have been triggered by the OSW due to the high temperature and pressure of the post-shock flow, but it is suppressed by the expansion waves due to a decrease in the pressure and temperature of the post-expansion waves. Therefore, the detonation is not initiated. Figure 8 shows the

corresponding pressure and temperature distribution along  $y = 12$  mm and  $y = 20$  mm, illustrating the location of the beginning of the interaction of the OSW and expansion wave. In the 10 mm wedge case, the peak pressure is less than the first stage value of 247 kPa due to the OSW for  $y = 12$  mm, which indicates that the beginning of the interaction is located upstream at the point (14.5 mm, 12 mm); for the other cases, it is located downstream. For  $y = 20$  mm, the peak pressure is similar with the peak pressure in induction zone at  $y = 12$  mm, which should have been attributed to the effects of the expansion waves, illustrating that the beginning of the interaction is located upstream at the transition point (22.5 mm, 20 mm). The expansion waves affect the detonation initiation. The deflagration wave and the shock wave are reduced, which means that a detonation cannot be established.

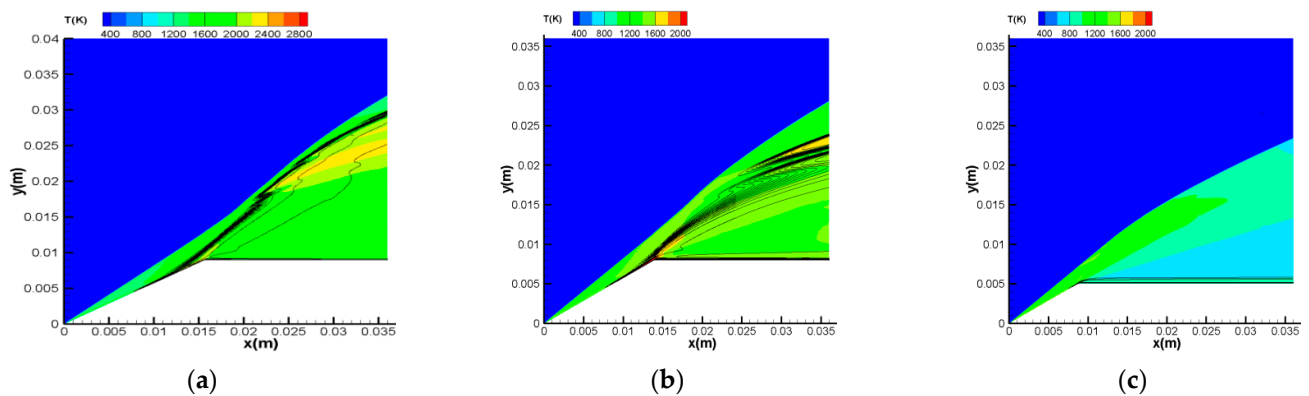


**Figure 7.** Contours of temperature and  $H_2O$  mass fraction (black lines) for the 18 mm wedge, 16 mm wedge and 10 mm wedge: (a) 18 mm wedge; (b) 16 mm wedge; (c) 10 mm wedge.

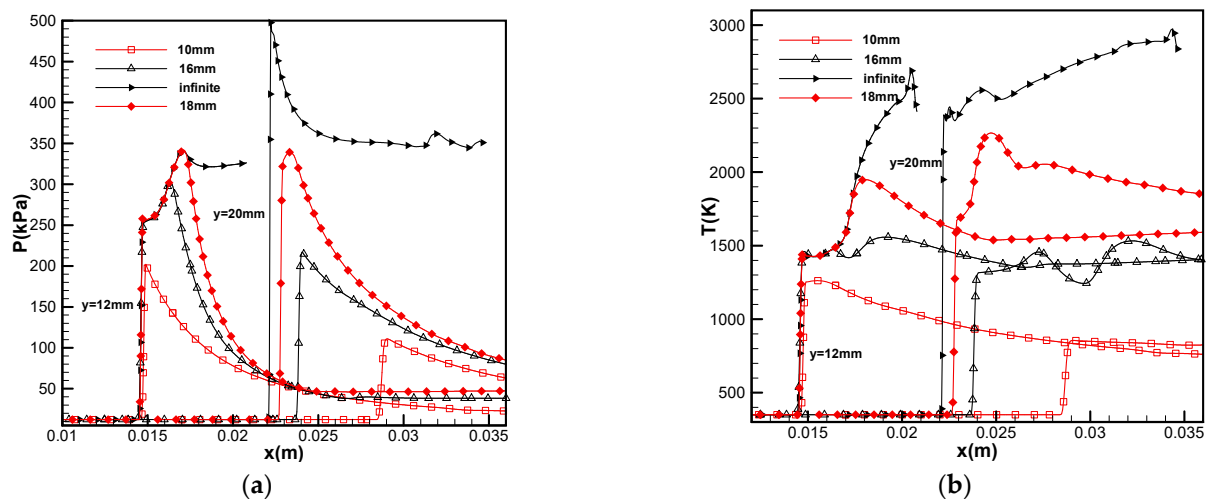


**Figure 8.** Pressure and temperature along  $y = 12$  mm and  $y = 20$  mm for the infinite wedge, 18 mm wedge, 16 mm wedge and 10 mm-wedge. (a) Pressure. (b) Temperature.

As the wedge length decreases, three combustion regimes, detonation, decoupled combustion and no ignition, can be subsequently observed. When the OSW–ODW transition point is on the wedge, as in the case of the 32 mm wedge, the expansion waves do not affect the evolution of the ODW, which may have been reduced far downstream, outside the computational domain in this paper. When the transition point is located downstream of the turning point of the wedge, as for the 24 mm wedge and 19 mm wedge, a detonation can be initiated, but it is decoupled downstream. When the wedge length is less than a critical value, as in the cases of the 18 mm wedge and 16 mm wedge, a detonation cannot be established and a decoupled combustion is formed. For a wedge length small enough, as in the case of the 10 mm wedge, a rapid reaction cannot be established, and the shock wave

decays due to the effects of the expansion waves, which is a finding similar to the results obtained by Papalexandris [29] and Fang et al. [31]. However, all the possible combustion regimes induced by finite wedges are obtained in this study.

### 3.3. Initiation Criterion of ODWs for Finite Wedges

As is indicated in Section 3.2, the expansion waves that originated from the turning point affect the downstream region and produce a decrease in the temperature and pressure, which delays the initiation of the reaction and results in a decoupled combustion. However, they do not affect the upstream region, and the upstream flow field is almost the same as that in the infinite case. The location of the beginning of the interaction of the shock wave and expansion wave is a key parameter for determining the expansion wave's effects on the detonation initiation. When the beginning of the interaction is located downstream of the transition point, the evolution of the ODW is not affected by the expansion and the ODW can be initiated. When the beginning of the interaction is located upstream of the transition point, the ODW cannot be initiated. Thus, when the beginning of the interaction is located at the transition point, it may have been the critical case, such as the 19 mm wedge case, shown in Figure 9a.

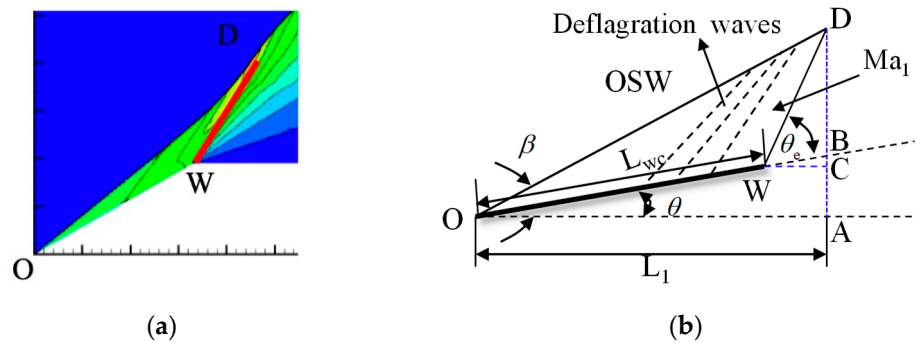


**Figure 9.** Sketch of OSW and expansion wave in the critical case (DW: expansion wave). (a) Pressure contours in the 19 mm wedge case. (b) Simplified wave structures.

The flow Mach number before the left expansion wave varies in a small range, and the angle of the left expansion wave changes within a small range. Thus, we can use an oblique line to represent the left expansion wave. Assuming that the left expansion wave produced from the turning point interacts with the shock wave at the transition point, a sketch of the shock wave and the expansion wave in the critical case is presented in Figure 9b. The line OD represents the OSW, i.e., the shock wave. The line OW is the wedge with the critical length  $L_{wc}$  and angle  $\theta$ . Line DW represents the left expansion wave.  $\beta$  is the shock wave angle, while  $\theta_e$  is the left expansion wave angle.  $L_1$  is the x coordinate of the transition point D. The wedge angle  $\theta$  was given previously, while  $\beta$  and  $L_1$  can be obtained from the infinite case. The Mach number  $Ma_1$  of the flow upstream DW can also be derived from the simulated infinite case, so  $\theta_e$  can be obtained using the following equation:

$$\theta_e = \arcsin\left(\frac{1}{Ma_1}\right) \tag{4}$$

Therefore, the parameters  $\theta$ ,  $\beta$ ,  $L_1$  and  $\theta_e$  are known, and the critical length  $L_{wc}$  can be obtained according to the relation of lines in Figure 9, expressed as

$$L_{wc} = \frac{L_1}{\cos \theta} - \frac{L_1 \tan \beta - L_1 \tan \theta}{\cos \theta \tan(\theta + \theta_e) - \sin \theta} \tag{5}$$

In Equation (5), the wedge angle  $\theta$  is given as the boundary condition, and the shock wave angle  $\beta$  can also be derived from the implicit relationship between the wedge angle  $\theta$  and the shock wave angle  $\beta$ , except for that from the simulation result.

$$\frac{\tan(\beta - \theta)}{\tan \beta} = \frac{2 + (\gamma - 1)Ma_0^2 \sin^2 \beta}{(\gamma + 1)Ma_0^2 \sin^2 \beta} \quad (6)$$

where  $\gamma$  is the inflow specific heat ratio.  $Ma_1$  and  $L_1$  are related to the inflow parameters and chemical reactions.  $Ma_1$  is the flow Mach number before the left expansion wave. The flow passes through the deflagration waves and the flow Mach number decreases with respect to the post-shock flow Mach number. Although the flow Mach number between the deflagration waves and the expansion waves varies within a small range, it has little influence on  $L_{wc}$ . Thus,  $Ma_1$  can be obtained using a point between the deflagration waves and the expansion waves in the infinite wedge simulation case shown in Figure 9b or the theoretical method in [19]. The  $x$  coordinate of the OSW–ODW transition point  $L_1$  is measured from the infinite wedge simulation results. The angle of the  $x$  axis and the wedge is the wedge angle  $\theta$ . If the  $x$  axis is parallel to the wedge,  $L_1$  should be obtained by coordinate transformation.

From the infinite wedge case, it can be found that  $\theta = 30^\circ$ ,  $\beta = 40^\circ$ ,  $L_1 = 22.5$  mm,  $Ma_1 = 2.13$  and  $\theta_e = 28^\circ$ ; thus,  $L_{wc} = 19$  mm. For the inflow conditions,  $Ma_0 = 6.5$ ,  $P_0 = 12.25$  kPa, and  $T_0 = 350$  K, and the critical wedge length is 19 mm. Figures 5d and 7a show the temperature contours and H<sub>2</sub>O mass fraction distribution for the 19 mm wedge and 18 mm wedge. The expansion waves quench the ODW for the 18 mm wedge. When the wedge length is less than 19 mm, the ODW cannot be initiated, indicating that the predicted critical length is correct.

The induction length defined by Xiang et al. [34] is 10.5 mm for this inflow condition, but the initiation of the ODW does not occur in the 16 mm wedge case, in which the wedge length  $L_w$  and the induction length  $L_c$  satisfy the relationship  $L_w > L_c$ . Thus, the initiation criterion proposed by Xiang is not suitable for the case in this paper.

### 3.4. Verification of the Initiation Criterion

To verify the initiation criterion, new cases are simulated. The inflow pressure  $P_0$  is changed to 40 kPa, while the other inflow parameters and the wedge angle remain unchanged. Figure 10 shows the temperature contours and the H<sub>2</sub>O mass fraction distribution for different wedge lengths. Three combustion regimes—detonation, decoupled combustion, and no auto-ignition—are also observed to take place sequentially as the wedge length decreases. When the wedge length is greater than 5 mm, the ODW is initiated, and the location of the transition point remains almost unchanged. When the wedge length is smaller than 5 mm, the ODW cannot be initiated. As the wedge length decreases to 3 mm, the gas remains almost non-reacted. For the inflow condition, it can be found from the infinite wedge case that  $\theta = 30^\circ$ ,  $\beta = 40^\circ$ ,  $L_1 = 5.5$  mm, and  $Ma_1 = 2.13$ , so the critical wedge length  $L_{wc} = 4.7$  mm, which agrees with the simulated results, illustrating that the predicted critical wedge length is correct.

Furthermore, for the 10 mm wedge, although the ODW is initiated and the incident shock wave is coupled with the reaction front downstream, there are obvious differences in the structures of the ODWs downstream. Figure 11 shows a comparison of the temperature contours for the 10 mm wedge and the infinite wedge. The ODW is fully developed prior to its interaction with the expansion waves. This interaction reduces the ODW strength and leads to the bending of the ODW, which seems to stop at the angle 42.4. This is close to the CJ detonation angle of 42° obtained by shock polar analysis, in which the CJ Mach number is 4.42, which was obtained by the CHEMKIN package [39]. Thus, the ODW is reduced to the CJ ODW downstream of the beginning of the interaction. This result is similar to those obtained by Papalexandris [29] and Walter and Silva [30], which indicates that the numerical results in this paper are reasonable.

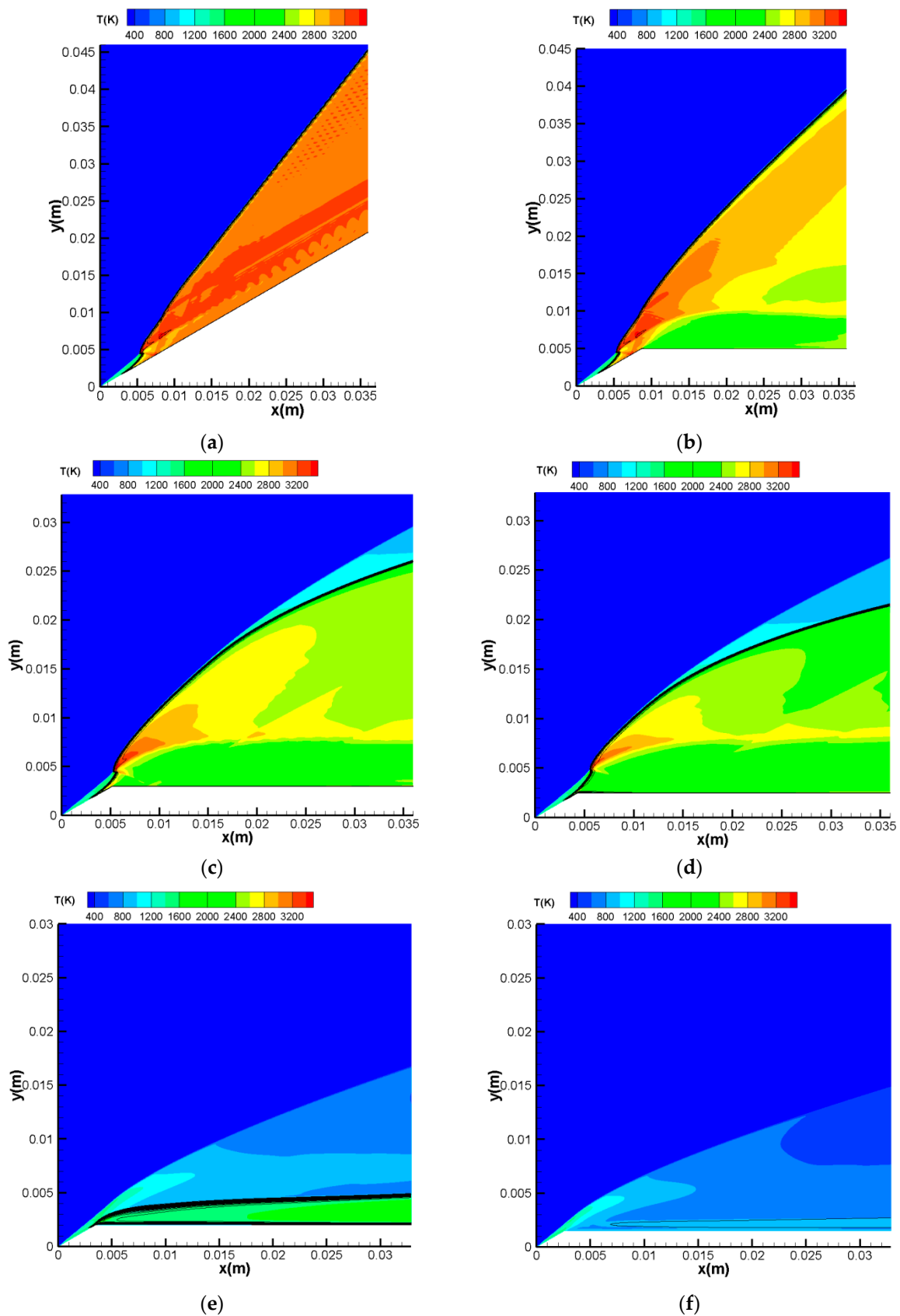


**Figure 10.** Contours of temperature and  $H_2O$  mass fraction (black lines) with different wedge lengths: (a) infinite wedge; (b) 10 mm wedge; (c) 6 mm wedge; (d) 5 mm wedge; (e) 4 mm wedge; (f) 3 mm wedge.

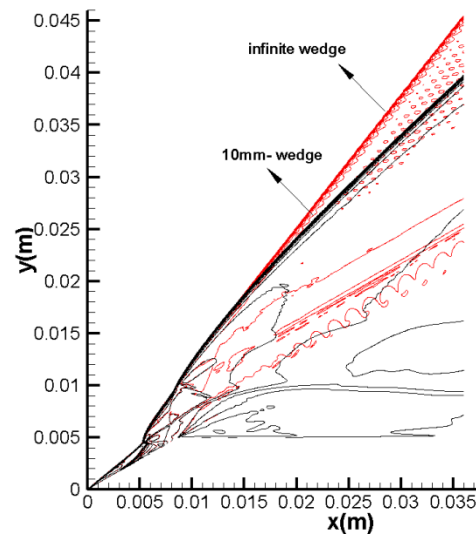


Figure 11. Comparison of temperature contours for the infinite wedge and 10 mm wedge.

To verify the criterion further, we analyze more cases with different Mach numbers and 40 kPa inflow pressure. Figure 12 presents the boundary of the initiation of detonation in different Mach numbers and wedge lengths. The hollow square denotes no detonations, and the solid square denotes detonations. The red triangle represents the critical wedge length obtained by Equation (5). The initiation of ODW can be accurately distinguished by the red triangle. Therefore, the critical wedge length can be used as a criterion to predict the initiation of ODW induced by a finite wedge.

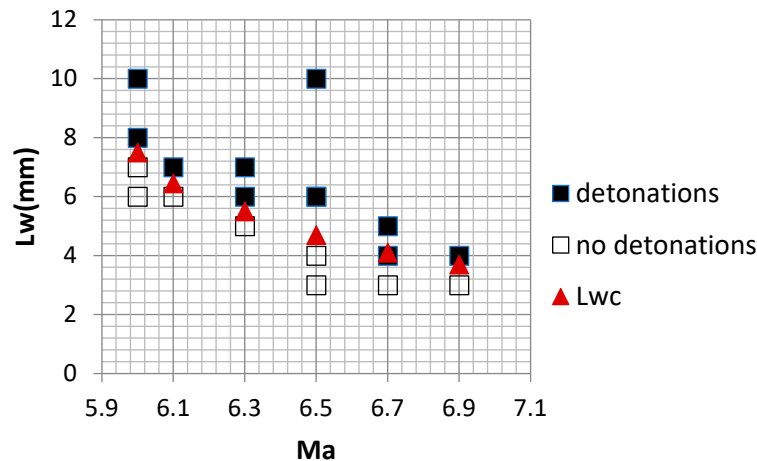
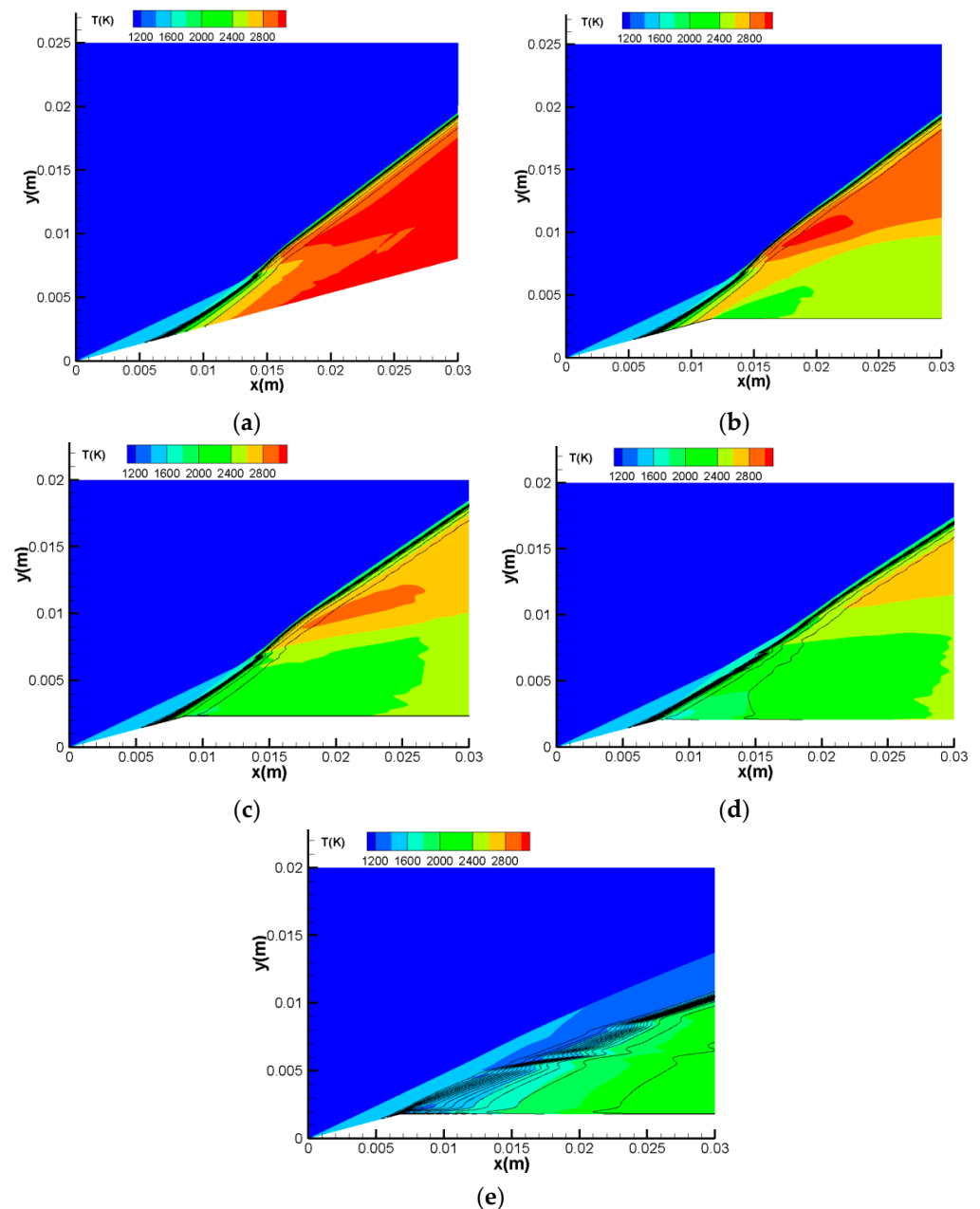


Figure 12. Characteristics of detonation initiation with different Mach numbers and wedge lengths.

The criterion proposed by Xiang et al. [34] cannot predict the critical wedge length for the inflow condition in Section 3.2. The inflow condition discussed by Xiang et al. [34] featured a high temperature in high altitude, which is different from the simulated cases in this paper. Thus, the cases studied by Xiang et al. [34] and Fang et al. [40] are also simulated in order to verify the criterion. The inflow conditions are  $Ma_0 = 4.3$ ,  $P_0 = 119$  kPa, and  $T_0 = 998$  K. The wedge angle is  $15^\circ$  and the uniform grid with a size of  $25 \mu\text{m}$  is employed. The OSW–ODW transition pattern is a smooth transition, as shown in Figure 12, and is similar to the results of Xiang et al. [34] and Fang et al. [40]. The ODW structure for the infinite wedge is similar to that obtained by Fang et al. [40], while there is some divergence in the location of the transition point compared with that recorded in Xiang et al. [34]. This may have been attributed to different detailed chemical models applied in both papers. From the infinite case, it is known that  $\theta = 15^\circ$ ,  $\beta = 26^\circ$ ,  $L_1 = 14.6$  mm, and  $Ma_1 = 2.7$ ; thus,

the critical wedge length  $L_{wc} = 8.2$  mm. When the wedge length is less than 8 mm, the ODW cannot be initiated, as shown in Figure 13. This indicates that the predicted critical wedge length is correct.



**Figure 13.** Contours of temperature and  $H_2O$  mass fraction (black lines) with different wedge lengths at high temperature in a high altitude: (a) infinite wedge; (b) 12 mm wedge; (c) 9 mm wedge; (d) 8 mm wedge; (e) 7 mm wedge.

#### 4. Conclusions

In this study, ODWs induced by finite wedges are simulated by Euler equations with a detailed chemistry model. This study examines the effects of expansion waves on the initiation of ODWs. As the wedge length decreases, three different combustion regimes, ODW, decoupled combustion, no ignition, are subsequently observed to occur. The expansion waves affect the flowfield downstream of the interaction region, while the upstream region is not influenced, and is almost the same with that in the infinite wedge case. The interaction decreases the pressure and temperature, leading to a progressive

bending of the ODW, which would reduce to a CJ detonation wave or decouple with a reaction front downstream. The location of the interaction point of the shock wave and the expansion wave is a key parameter for the detonation initiation.

The critical wedge length can be derived from the relationship of the OSW, the expansion wave and the ODW. Then, the initiation criterion of the ODW for the finite wedge can be proposed. When the wedge length is greater than the critical wedge length, an ODW can be initiated. When the wedge length is smaller than the critical wedge length, the initiation of the ODW cannot be established. For wedge lengths small enough, no ignition occurs. The initiation criterion can accurately predict the detonation initiation with different Mach numbers and inflow pressures. Compared with previously proposed criteria, the criterion in this study is predicted to perform better.

**Author Contributions:** Conceptualization, J.Q.; Methodology, J.Q. and D.Z.; Software, J.Q.; Validation, J.Q.; Formal analysis, J.Q.; Investigation, J.Q.; Resources, D.Z.; Data curation, J.Q.; Writing—original draft preparation, J.Q.; Writing—review and editing, J.Q.; Visualization, J.Q.; Supervision, D.Z.; Project administration, D.Z.; Funding acquisition, D.Z. All authors have read and agreed to the published version of the manuscript.

**Funding:** This research was funded by National Natural Science Foundation of China, grant number 11872350 and Defense Industrial Technology Development Program JCKY2020110B034.

**Data Availability Statement:** All data used during the study appear in the submitted article.

**Acknowledgments:** We thank Wubing Yang and Ming Yan for the suggestions of analyzing the results.

**Conflicts of Interest:** The authors declare no conflict of interest.

## References

1. Kailasanath, K. Recent developments in the research on pulse detonation engines. *AIAA J.* **2003**, *41*, 145–159. [[CrossRef](#)]
2. Wokanski, P. Detonation propulsion. *Proc. Combust. Inst.* **2013**, *34*, 125–158. [[CrossRef](#)]
3. Zhang, Z.; Ma, K.; Zhang, W.; Han, X.; Liu, Y.; Jiang, Z. Numerical investigation of a Mach 9 oblique detonation engine with fuel pre-injection. *Aerosp. Sci. Technol.* **2020**, *105*, 106054. [[CrossRef](#)]
4. Ma, J.Z.; Zhang, S.; Luan, M.; Wang, J. Experimental investigation on delay time phenomenon in rotating detonation engine. *Aerosp. Sci. Technol.* **2019**, *88*, 395–404. [[CrossRef](#)]
5. Pratt, D.T.; Humphrey, J.W.; Glenn, D.E. Morphology of standing oblique detonation waves. *J. Propuls. Power* **1991**, *7*, 837–845. [[CrossRef](#)]
6. Grismer, M.J.; Powers, J.M. Numerical prediction of oblique detonation stability boundaries. *Shock Waves* **1996**, *6*, 147–156. [[CrossRef](#)]
7. Powers, J.M.; Gonthier, K.A. Reaction zone structure for strong, weak overdriven, and weak underdriven oblique detonations. *Phys. Fluids* **1992**, *4*, 2082–2089. [[CrossRef](#)]
8. Powers, J.M.; Stewart, D.S. Approximate solutions for oblique detonations in the hypersonic limit. *AIAA J.* **1992**, *30*, 726–736. [[CrossRef](#)]
9. Morris, C.I.; Kamel, M.R.; Hanson, R.K. Shock-induced combustion in high-speed wedge flows. *Proc. Combust. Inst.* **1998**, *27*, 2157–2164. [[CrossRef](#)]
10. Li, C.; Kailasanath, K.; Oran, E.S. Detonation structures behind oblique shocks. *Phys. Fluids* **1994**, *4*, 1600–1611. [[CrossRef](#)]
11. Vlasenko, V.V.; Sabelnikov, V.A. Numerical simulation of inviscid flows with hydrogen combustion behind shock waves and in detonation waves. *Combust. Explos. Shock Wave* **1995**, *31*, 376–389. [[CrossRef](#)]
12. Viguier, C.; da Silva, L.F.F.; Desbordes, D.; Deshaies, B. Onset of oblique detonation waves: Comparison between experimental and numerical results for hydrogen-air mixtures. *Symp. (Int.) Combust.* **1996**, *26*, 3023–3031. [[CrossRef](#)]
13. Broda, J.C. An Experimental Study of Oblique Detonation Waves. Ph.D. Thesis, Connecticut University, Storrs, CT, USA, 1993.
14. da Silva, L.F.F.; Deshaies, B. Stabilization of an oblique detonation wave by a wedge: A parameter numerical study. *Combust. Flame* **2013**, *121*, 152–166. [[CrossRef](#)]
15. Teng, H.H.; Jiang, Z.L. On the transition pattern of the oblique detonation structure. *J. Fluid Mech.* **2012**, *713*, 659–669. [[CrossRef](#)]
16. Wang, A.F.; Zhao, W.; Jiang, Z.L. The criterion of the existence or inexistence of transverse shock wave at wedge supported oblique detonation wave. *Acta Mech. Sin.* **2011**, *27*, 611–619. [[CrossRef](#)]
17. Miao, S.; Zhou, J.; Liu, S.; Cai, X. Formation mechanism and characteristics of transition patterns in oblique detonations. *Acta Astronaut.* **2018**, *142*, 121–129. [[CrossRef](#)]
18. Qin, Q.Y.; Zhang, X.B. Study on the transition patterns of the oblique detonation wave with varying temperature of the hydrogen-air mixture. *Fuel* **2020**, *274*, 117827. [[CrossRef](#)]

19. Shi, X.; Xie, H.; Zhou, L.; Zhang, Y. A theoretical criterion on the initiation type of oblique detonation waves. *Acta Astronaut.* **2022**, *190*, 342–348. [[CrossRef](#)]
20. Teng, H.H.; Zhang, Y.N.; Jiang, Z.L. Numerical investigation on the induction zone structure of the oblique detonation waves, *Comput. Fluids* **2014**, *95*, 127–131.
21. Liu, Y.; Wu, D.; Yao, S.; Wang, J. Analytical and numerical investigations of wedge-induced oblique detonation waves at low inflow Mach number. *Combust. Sci. Technol.* **2015**, *187*, 843–856. [[CrossRef](#)]
22. Liu, Y.; Wu, D.; Wang, J.-P. Structure of an oblique detonation wave induced by a wedge. *Shock Waves* **2016**, *26*, 161–168. [[CrossRef](#)]
23. Yang, P.F.; Teng, H.H.; Jiang, Z.L.; Dick, N.H. Effects of inflow Mach number on oblique detonation initiation with a two-step induction-reaction kinetic model. *Combust. Flame* **2018**, *193*, 246–256. [[CrossRef](#)]
24. Yang, L.; Yue, L.; Zhang, Q.; Zhang, X. Numerical study on the shock/combustion interaction of oblique detonation waves. *Aerosp. Sci. Technol.* **2020**, *104*, 105938. [[CrossRef](#)]
25. Teng, H.; Tian, C.; Zhang, Y.; Zhou, L.; Ng, H.D. Morphology of oblique detonation wave in a stoichiometric hydrogen-air mixture. *J. Fluid Mech.* **2021**, *913*, A1. [[CrossRef](#)]
26. Teng, H.; Ng, H.D.; Yang, P.; Wang, K. Near-field relaxation subsequent to the onset of oblique detonations with a two-step kinetic model. *Phys. Fluids* **2021**, *33*, 096106. [[CrossRef](#)]
27. Zhang, G.Q.; Li, G.X.; Wang, K.L. Wave structure of oblique detonation disturbed by an expansion wave from a bended tunnel. *Appl. Therm. Eng.* **2020**, *180*, 115856. [[CrossRef](#)]
28. Choi, J.Y.; Shin, E.J.R.; Jeung, I.S. Unstable combustion induced by OSWs at the non-attaching condition of the oblique detonation wave. *Proc. Combust. Inst.* **2009**, *32*, 2387–2396. [[CrossRef](#)]
29. Papalexandris, M.V. A numerical study of wedge-induced detonations. *Combust. Flame* **2000**, *120*, 526–538. [[CrossRef](#)]
30. Walter, M.T.; da Silva, L.F.F. Numerical study of detonation stabilization by finite length wedges. *AIAA J.* **2006**, *44*, 353–361. [[CrossRef](#)]
31. Fang, Y.S.; Hu, Z.M.; Teng, H.H. Numerical investigation of oblique detonations induced by a finite wedge in a stoichiometric hydrogen-air mixture. *Fuel* **2018**, *234*, 502–507. [[CrossRef](#)]
32. Xiang, G.; Li, H.; Cao, R.; Chen, X. Study of the features of oblique detonation induced by a finite wedge in hydrogen-air mixtures with varying equivalence ratios. *Fuel* **2020**, *264*, 116854. [[CrossRef](#)]
33. Zhang, G.Q.; Gao, S.F.; Xiang, G.X. Study on initiation mode of oblique detonation induced by a finite wedge. *Phys. Fluids* **2021**, *33*, 016102. [[CrossRef](#)]
34. Xiang, G.; Li, X.; Sun, X.; Chen, X. Investigations on oblique detonations induced by a finite wedge in high altitude. *Aerosp. Sci. Technol.* **2019**, *95*, 105451. [[CrossRef](#)]
35. Liu, Y.; Han, X.; Yao, S.; Wang, J. A numerical investigation of the prompt oblique detonation wave sustained by a finite-length wedge. *Shock Waves* **2016**, *26*, 729–739. [[CrossRef](#)]
36. Li, C.; Kailasanath, K.; Oran, E.S. Effects of boundary layers on oblique-detonation structures. In Proceedings of the 31st Aerospace Sciences Meeting, Reno, NV, USA, 11–14 January 1993; p. 450.
37. Balakrishnan, G.; Williams, F.A. Turbulent combustion regimes for hypersonic propulsion employing hydrogen-air diffusion flames. *J. Propuls. Power* **1994**, *10*, 434–437. [[CrossRef](#)]
38. Guo, H.; Jia, X.; Zhao, N.; Li, S.; Zheng, H.; Sun, C.; Chen, X. The formation and development of oblique detonation wave with different chemical reaction models. *Aerosp. Sci. Technol.* **2021**, *117*, 106964. [[CrossRef](#)]
39. Kee, R.J.; Rupley, F.M.; Meeks, E.; Miller, J.A. *Chemkin-II: A Fortran Chemical Kinetics Package for the Analysis of Gas-Phase Chemical and Plasma Kinetics*; UC-405, SAND96-8216; Sandia National Laboratories: Livermore, CA, USA, 1996.
40. Fang, Y.; Hu, Z.; Teng, H.; Jiang, Z.; Ng, H.D. Numerical study of inflow equivalence ratio inhomogeneity on oblique detonation formation in hydrogen-air mixtures. *Aerosp. Sci. Technol.* **2017**, *71*, 256–263. [[CrossRef](#)]

**Disclaimer/Publisher’s Note:** The statements, opinions and data contained in all publications are solely those of the individual author(s) and contributor(s) and not of MDPI and/or the editor(s). MDPI and/or the editor(s) disclaim responsibility for any injury to people or property resulting from any ideas, methods, instructions or products referred to in the content.